Structure of Functional *Staphylococcus aureus* α-Hemolysin Channels in Tethered Bilayer Lipid Membranes

Duncan J. McGillivray,[†‡] Gintaras Valincius,[¶] Frank Heinrich,[†‡] Joseph W. F. Robertson,[‖] David J. Vanderah,[††] Wilma Febo-Ayala,[††] Ilja Ignatjev,[¶] Mathias Lösche,[†‡§*] and John J. Kasianowicz[‖]

[†]National Institute of Standards and Technology (NIST) Center for Neutron Research, Gaithersburg, Maryland; [‡]Physics Department and, [§]Department of Biomedical Engineering, Carnegie Mellon University, Pittsburgh, Pennsylvania; [¶]Institute of Biochemistry, Vilnius, Lithuania; [‖]Semiconductor Electronics Division, NIST, Electronics and Electrical Engineering Laboratory, Gaithersburg, Maryland; and [††]Biochemical Sciences Division, NIST, Chemical Sciences and Technology Laboratory, Gaithersburg, Maryland

ABSTRACT We demonstrate a method for simultaneous structure and function determination of integral membrane proteins. Electrical impedance spectroscopy shows that *Staphylococcus aureus* α-hemolysin channels in membranes tethered to gold have the same properties as those formed in free-standing bilayer lipid membranes. Neutron reflectometry provides high-resolution structural information on the interaction between the channel and the disordered membrane, validating predictions based on the channel's x-ray crystal structure. The robust nature of the membrane enabled the precise localization of the protein within 1.1 Å. The channel's extramembranous cap domain affects the lipid headgroup region and the alkyl chains in the outer membrane leaflet and significantly dehydrates the headgroups. The results suggest that this technique could be used to elucidate molecular details of the association of other proteins with membranes and may provide structural information on domain organization and stimuli-responsive reorganization for transmembrane proteins in membrane mimics.

INTRODUCTION

The primary goal of structural biology is to understand the structure-function relationship of proteins, which constitute the machinery of life. Despite the stunning achievements in determining protein structures using electron microscopy (1) and x-ray crystallography (2), the number of solved membrane protein structures significantly lags that of soluble proteins (3), in part because of the inherent difficulty of crystallizing proteins whose native environment is a disordered fluid membrane. Furthermore, these methods do not demonstrate whether the structural models are functionally accurate. NMR provides dynamic information about protein structure (4) but the technique is still limited to the study of relatively small proteins (i.e., with molecular mass <50 kDa) (5). Neutron reflectometry can provide complementary information to NMR and crystallography if a suitable interface for membrane protein reconstitution can be developed. The challenge lies in fabricating a biomimetic interface that retains the fluidity of a cell wall while providing long-term stability that is needed for structural characterization methods.

Tethered bilayer lipid membranes (tBLMs) combine the fluidity of a lipid bilayer with a stable platform for analysis with analytical techniques, including electrochemistry (6,7) and surface-sensitive scattering (8). Synthetic chemistry has recently been developed (8,9) that facilitates the formation of tBLMs in which the membranes are intrinsically disordered, thus permitting the reconstitution of proteins such as ion channels (10). Such membrane platforms are sufficiently resilient to be long-term stable (10,11) and can be characterized with neutron reflection at high resolution (8,12) by taking advantage of the possibility, offered by tBLM systems, to vary isotopic contrast and incorporate proteins in situ. This enables the acquisition of data sets before and after protein reconstitution, and under different isotopic labeling schemes, from one physical sample.

Although α-hemolysin (α-HL) spontaneously forms ion channels in free-standing bilayer lipid membranes (BLMs) (13), it is more difficult to reconstitute it into surface-bound membranes, presumably because of the rigidity of the membranes' inner leaflets (14). With a novel synthetic approach to tBLM synthesis, successful reconstitution of the membrane channels was recently demonstrated (10). In this work, we prepared a mixed self-assembled monolayer (SAM) of a thiahexa(ethylene oxide)-substituted lipid analog, 20-tetradecyloxy-3,6,9,12,15,18,22-heptaoxahexatricontane-1-thiol (WC14) (8) and β-mercaptoethanol (β-ME), then completed the bilayer with phospholipid via rapid solvent exchange (see Methods). Electrochemical impedance spectroscopy (EIS) and neutron reflection (NR) show that the resultant tBLMs are impermeable to ions and contain water in the submembrane space (8), which should facilitate protein reconstitution (7,15).

MATERIALS AND METHODS

Materials

WC14 was synthesized, purified, and characterized in house, as reported previously in the Supplementary Material of McGillivray et al. (8).

Submitted August 12, 2008, and accepted for publication November 18, 2008.

Duncan J. McGillivray and Gintaras Valincius contributed equally to this work.

*Correspondence: quench@cmu.edu

Duncan J. McGillivray's present address is Dept. of Chemistry, The University of Auckland, Auckland, New Zealand.

Wilma Febo-Ayala's present address is Dept. of Chemistry, University of Pennsylvania, Philadelphia, PA.

Editor: Thomas J. McIntosh.

0006-3495/09/02/1547/7 $2.00

doi: 10.1016/j.bpj.2008.11.020

1,2-diphytanoyl-*sn*-glycero-3-phosphatidylcholine (DPhyPC) and pyridyl–dithiopropionate-poly(ethylene glycol)-distearoyl-*sn*-glycerophosphatidyl-ethanolamine (PDP-PEG2000-DSPE) were from Avanti Polar Lipids (Birmingham, AL). β-ME (Sigma-Aldrich, St. Louis, MO) was distilled before use. Poly(ethylene glycol) (PEG) and D_2O (99.9% isotope purity) were obtained from Fluka (Ronkonkoma, NY) and Cambridge Isotopes Laboratory (Andover, MA), respectively. H_2O was from a Millipore (Billerica, MA) UHQ reagent-grade water purification system.

Conductance measurements of α-HL in free-standing bilayer membranes

Freestanding BLMs (16) were formed from DPhyPC on ~100 μm diameter holes in a thin Teflon partition separating two identical Teflon chambers (17) that each held ~2 mL of electrolyte solution (0.1 M KCl, 5 mM 3-(*N*-morpholino) propanesulfonic acid (MOPS), 5 mM 2-(*N*-morpholino) ethanesulfonic acid (MES) at either pH 7.5 or 4.5). A small voltage (~2 mV) was applied across the membrane via two matched Ag/AgCl electrodes, and the ionic current was converted to voltage and amplified with an Axon Instruments 200B patch clamp amplifier (Molecular Devices, Sunnyvale, CA) in the voltage clamp mode. α-HL channels were formed by adding the toxin to one chamber while briefly stirring the solution.

Surface preparation

The chemicals used are described in the Supporting Material. SAMs were formed on thin gold layers (~100 Å for neutron reflectivity NR, ~2000 Å for EIS), deposited by direct current magnetron sputtering (Auto A306; BOC Edwards, Crawley, West Sussex, UK) on [100]-cut Si wafers precoated with an ~20 Å thick Cr adhesion layer. The gold films typically had an RMS surface roughness of ~5 Å, as measured by x-ray reflectometry (Bruker AXS, Madison, WI), and a uniformity of thickness across the surface of $\pm$ 3% or better, as determined by ellipsometry.

We demonstrated in recent work that the dilution of tether points in tBLMs, for example with β-ME, is essential for the formation of fluid bilayers in tBLMs that incorporate a ~2 nm thick hydrated cushion between the membrane and the solid support (8). Mixed SAMs were prepared by exposing magnetron-sputtered Au films to solutions of WC14: β-ME (3:7 mol/mol, 0.2 mM total concentration) in 99.5% ethanol for >12 h. Because of the short hexa(ethylene oxide) tether, these SAMs and completed tBLMs incorporate hydrated submembrane layers that are only 15 Å thick (8,18,19). The tBLMs were subsequently completed by incubation of the moderately hydrophobic surface with a concentrated (~10 mM) DPhyPC solution that was rapidly, within ~5 s, replaced by vigorous injection of aqueous buffer (0.1 M NaCl, 0.005 M NaH_2PO_4/Na_2HPO_4, pH 7.5) into the sample cell. This rapid solvent exchange procedure leads to the formation of complete and electrically insulating bilayers (8). The tBLMs used here had residual specific conductances <3 μS cm^{-2}. Because of this low background conductance, the tBLMs were well suited to detect toxin-induced membrane conductance changes. tBLMs that incorporated longer tethers, providing a thicker hydrated submembrane layer, were prepared by chemisorption of SAMs from PDP-PEG2000-DSPE without β-ME, followed by solvent exchange. Solutions with different pH values used in EIS were of the same buffer composition. However, the solvent exchange was always carried out at pH 7.5.

Electrochemical impedance spectroscopy

EIS measurements were performed using an electrochemical impedance system (Solartron Analytical, Farnborough, Hampshire, UK, model 1287 potentiostat, model 1252A frequency response analyzer and software). The spectra were obtained for frequencies between 1 and 6.5×10^4 Hz with 10 logarithmically distributed measurements per decade. Six electrochemical cells were assembled on a 20×40 mm large gold-coated silicon wafer used as the working electrode that had the tBLMs attached to its surface. Each of these six parallel cells had an effective real surface area of 0.44 cm^2. The reference was a saturated silver-silver chloride (Ag/AgCl/NaCl(aq,sat)) microelectrode (M-401F, Microelectrodes, Inc., Bedford, NH), and the auxiliary electrode was a 0.5 mm diameter platinum wire (Aldrich, St. Louis, MO, 99.99% purity) coiled around the barrel of the reference electrode. All measurements were carried out at 0 V direct current bias versus reference electrode at T = (21 $\pm$ 1)°C.

Neutron reflectivity measurements and data modeling

NR was measured on the Advanced Neutron Diffractometer/Reflectometer (12) at the National Institute of Standards and Technology Center for Neutron Research. tBLMs were sufficiently robust to permit the injection of aqueous buffers of various isotopic compositions into the sample chamber and sequentially collect NR spectra that each take ~6 h. After the bare tBLM was characterized at different solvent contrasts, ~1 μM α-HL (final concentration) was injected into the sample cell in D_2O-based buffer and equilibrated with the membrane for 6 h. Finally, the protein-reconstituted tBLM was examined in protein-free buffers of various isotopic compositions. The total experiment time exceeded 36 h, during which the tBLM was stable.

Data analysis was performed in terms of homogeneous layer models, or "box" models (20), using the *ga_refl* software developed at the NIST Center for Neutron Research (21). The reflectivity due to a model neutron scattering length density (nSLD) profile was computed using an optical matrix based on Parratt's recursion algorithm (22). Isostructural samples with distinct isotopic contrast were fitted simultaneously by consistently refining the corresponding nSLD profiles that were parameterized in terms of the underlying molecular structures (23,24). The robustness of the tBLMs permitted the characterization of the membrane at various solvent contrasts followed by protein reconstitution and further NR characterization of the reconstituted tBLM with the same physical sample without removal from the reflectometer. With the substrate and membrane structures thus established, the structural changes due to protein incorporation could be studied in full detail. Although the data at the highest momentum transfer ($Q_z > 0.2$ Å^{-1}) do not appear to contribute information about distinctive structural features of the tBLM with and without the protein (see Fig. 3 below and the Supporting Material), these data were included in the error-weighted fitting because they contribute information about the overall sample structure.

For a refined data analysis, the crystal structure of the α-HL channel (Protein Data Bank accession code: 7AHL) (25) was incorporated into the model by assuming that the barrel of the protein was aligned perpendicular to the membrane (z direction) and the crystal structure was undisturbed. The contribution of the protein to the nSLD profile along z was then divided into 0.5 Å thick slices in which the sums of the atomic scattering lengths, divided by the solvent-excluded volumes, were calculated. The solvent-excluded volume was determined by the method of Connolly (26), using a 1.4 Å radius probe to represent a water molecule. In the fitting to the data, the resultant protein nSLD contribution was allowed to shift freely along z relative to the bilayer membrane. The lateral protein density at/in the membrane was accounted for as a fitting parameter. Protein contributions in the aqueous volume phase outside the membrane slabs were integrated into six layers. Measurements were typically made in three solvent contrasts (D_2O, H_2O, and a D_2O/H_2O mixture with an nSLD of 4×10^{-6} Å^{-2}, "CM4"). All solvent contrasts were simultaneously fitted for the tBLM with and without α-HL (21).

RESULTS AND DISCUSSION

Electrochemical investigation of biomimetic interface and of protein functionality

The addition of α-HL to the aqueous phase caused significant changes in the magnitude of the tBLM impedance, $|Z|$, and the phase angle (Fig. 1). These EIS features are associated with ion flux induced by membrane ionophores (6). Quantitative information was obtained by modeling the

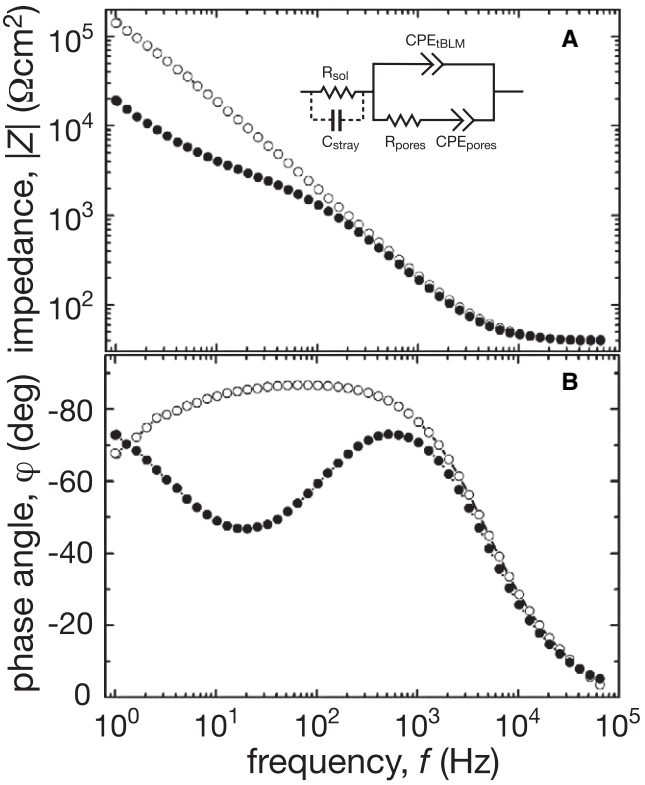

FIGURE 1 EIS spectra of a tBLM before and after α-HL reconstitution. The Bode plots (*A*) and phase angles (*B*) were measured with tBLMs in 0.1 M NaCl, 5 mM phosphate buffer at pH 7.5 before (*open circles*) and 2 h after the addition of α-HL to a final concentration of 50 nM (*solid circles*). The temperature was (21 ± 1)°C. The data were normalized with respect to the membrane surface area. (*Inset*) Equivalent model circuit for the tBLM.

impedance spectra with the equivalent circuit shown in Fig. 1 *A* (for details of the fitting, see the Supporting Material). The membrane is characterized by a constant phase element (CPE_{tBLM}) (27), with $\alpha = 0.986 \pm 0.001$ ($n = 22$ samples), which suggests a nearly ideal capacitive behavior of the electrically insulating dielectric bilayer (14). The CPE_{tBLM} coefficient, $(0.62 \pm 0.01)\ \mu F \times cm^{-2}\ s^{(\alpha-1)}$ ($n = 22$ samples), agrees with the specific capacitance values for solvent-free BLMs (28). Upon incubation with α-HL, CPE_{tBLM} increases in a protein concentration- and time-dependent manner, which suggests a net increase in the bilayer dielectric constant upon insertion of water-filled ion channels into the membrane (29). In addition, the reconstitution of ion channels creates parallel conductance pathways that bypass the membrane's high resistance. These pathways are represented by another constant phase element, CPE_{pores}, in series with a resistor, R_{pores}. The nearly ohmic open channel conductance determines R_{pores}, whereas CPE_{pores} is determined by a complex combination of the conductance of the aqueous reservoir between the Au surface and the inner membrane and the differential capacitance of the Au/reservoir interface.

Several criteria were used to demonstrate that the α-HL channels in the tBLMs were equivalent to those in free-standing BLMs. First, the toxin increased the tBLM conductance in proportion to both the bulk electrolyte conductivity and the ion (i.e., the conductance is greater in a KCl than in an NaCl solution), as it does in BLMs (13) (data not shown). Second, the rates at which α-HL increased the conductance of tBLMs correlated with those of free-standing BLMs at the same pH values (Fig. 2 *A*). Third, the conductance

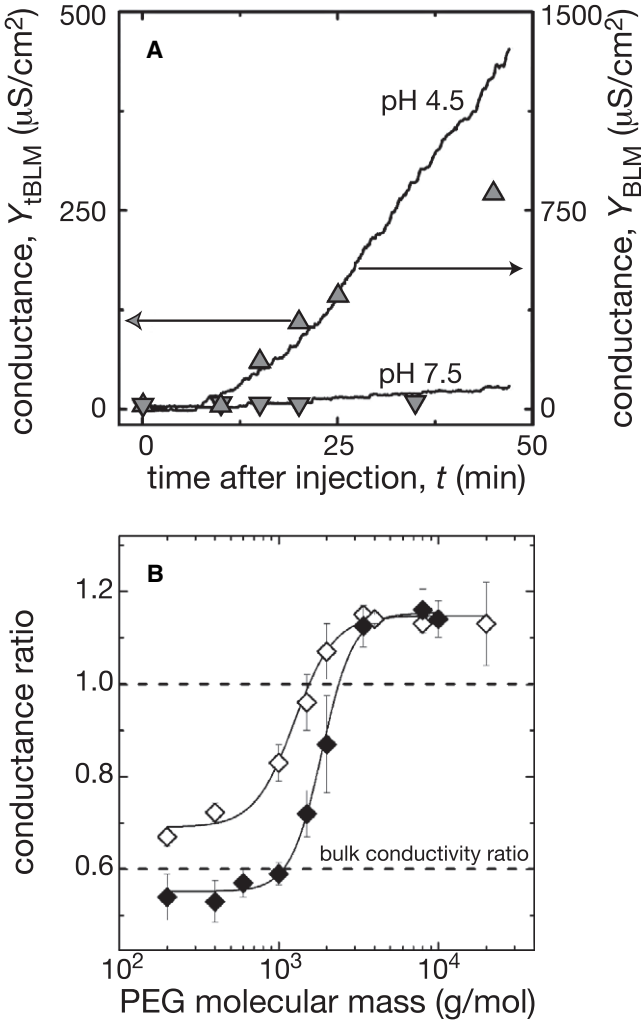

FIGURE 2 (*A*) Kinetics of α-HL channel formation in free-standing and tethered bilayer lipid membranes. The rate at which α-HL increased the specific conductance of tBLMs was greater at pH 4.5 (*up triangles*) than at pH 7.5 (*downward triangles*). Similar results were obtained with free-standing BLMs (*solid lines*). The applied potential was 10 mV alternating current (tBLM) and 2 mV direct current (BLM). In the BLM experiments, α-HL was added to the solution bathing one side of the membrane. In both experiments, the bulk concentration of α-HL was 50 nM. For the EIS data, the model-derived conductance, $Y_{\alpha\text{-HL}} = {R_{pores}}^{-1}$, was normalized with respect to the surface area. (*B*) Effect of size-selected PEGs on α-HL channel conductance. Polymers with molecular mass ≤2000 g/mol decreased the conductance of tBLMs containing many α-HL channels (*open diamonds*) and of single α-HL channels in a free-standing BLM (*solid diamonds*) (30). The concentration of PEG in each experiment was 15% (w:w). The curves are drawn to guide the eye. The bottom dashed line indicates the ratio of the bulk conductivities, σ(+PEG)/σ(−PEG).

increased superlinearly with the bulk α-HL concentration in both membrane types (data not shown). In general, the specific conductance increases induced by α-HL in tBLMs were within an order of magnitude (usually within a factor of 2 to 7) of those in free-standing BLMs.

The diameter of the α-HL channel in free-standing BLMs was estimated previously from the effect of PEG on the channel conductance (30). The conductance decreases when the PEGs are small enough to partition into the pore. For α-HL, this limit is ~2250 g/mol. Fig. 2 *B* shows that the effect of different molecular mass PEGs on the conductance of α-HL-doped tBLMs (*open symbols*) is similar to that on single α-HL channels in free-standing BLMs (*solid symbols*). The difference between the two partitioning plots might be due to restricted diffusion of PEG in the region adjacent to the Au electrode on the solid surface. Nevertheless, the results suggest that the values of the conductance, $Y_{\alpha\text{-HL}} = {R_{\text{pores}}}^{-1}$, derived from the EIS model are directly related to the intrinsic conductance of α-HL.

The correspondence between the results in BLMs and tBLMs demonstrates that α-HL channels are functional in both systems. Thus, other techniques such as NR can be used to determine the structural characteristics of the α-HL-membrane complex, taking advantage of the tBLM system's high stability.

Neutron reflectometry of the biomimetic interface

The sample preparation led to a robust film that was stable for days and survived solvent exchanges for isomorphic contrast adjustments (12). The multiple solvent contrasts allow for unambiguous determination of model parameters. For details of the technique, see Majkrzak et al. (31) and references therein. Fig. 3 shows NR results for a tBLM with and without α-HL in D_2O (for full data sets, see the Supporting Material). Changes in the scattering after exposure to α-HL are shown as error-weighted residuals of reflectivity data against the best-fit reflectivity model of the protein-free tBLM. Deviations from the baseline are most pronounced at low momentum transfer (e.g., around $Q_z = 0.05$ Å^{-1}, where the coordinate z is normal to the membrane plane and originates at the gold/thiol interface). This indicates significant structural changes of the bilayer upon α-HL reconstitution on the length scale, $2\pi/Q_z \approx 120$ Å, the approximate height of the α-HL channel along its symmetry axis (25). Although less pronounced than those around $Q_z = 0.05$ Å^{-1}, significant deviations persist to 0.2 Å^{-1}. However, more information can be extracted from these data sets by using more detailed fitting of the data, with additional details gleaned from the use of multiple solvent contrasts.

Simultaneously fitting the data in three solvent contrasts to a slab model with a single extramembranous layer accounts for the most prominent feature of the channel: its large cap domain exterior to the membrane (25). Structural details were derived from a composition-space model (23,24) of

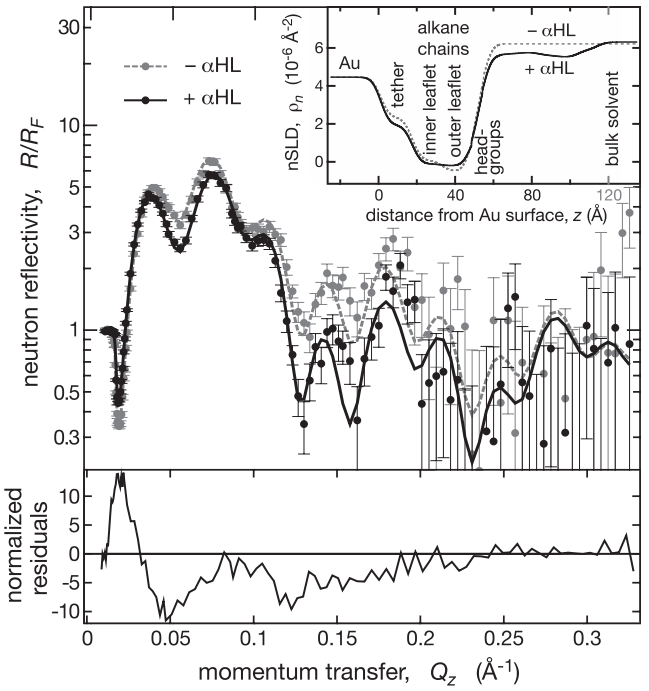

FIGURE 3 NR of protein-free and protein-reconstituted tBLMs. Before exposure to α-HL, the tBLM was characterized at two solvent contrasts (for data and modeled nSLD profiles, see Figs. S3 and S4, respectively, in the Supporting Material). Nine-hundred nanomoles of α-HL were subsequently injected into the sample cell in D_2O-based buffer and equilibrated with the membrane for 6 h. The protein-reconstituted tBLM was finally examined in protein-free buffers of various isotopic compositions. (*Main panel*) Fresnel-normalized NR of the tBLM in D_2O-based buffer before and after α-HL reconstitution. (*Bottom panel*) Because all data sets derive from the same physical sample, an error-weighted residuals plot shows exactly the protein contributions to the reflectivity. (*Inset*) nSLD profiles derived for the data in the main panel from a simultaneous fit to five data sets. Only the outer 30 Å of the inorganic surface structure of the solid substrate are shown. The nSLD profiles in the inset yield the reflectivity models shown as continuous lines in the main panel.

the membrane-inserted α-HL array. This modeling procedure assumes the protein inserts into the membrane according to its known x-ray structure (25) and suggests that the nanopore spans the tBLM with its β-barrel stem end flush with the lipid headgroup region of the inner bilayer leaflet (Fig. 4, tabulated details can be found in the Supporting Material). Although this is not obvious from the nSLD profile (Fig. 4 *A*), the optimized parameter set determines the penetration depth to within ± 1.1 Å, as shown in Fig. 5 *A* by a rigorous evaluation of parameter confidence limits with a Monte Carlo resampling technique (Supporting Material). The α-HL stem is thus located ~15 Å away from the Au interface. Control experiments with α-HL in a tBLM prepared with a longer tether (i.e., 60 Å) indicated that the proximity of the Au surface to the WC14-based tBLM does not alter the association of α-HL with the membrane (Supporting Material).

A quantitative evaluation of the nSLD profile shows that the α-HL channel reconstitutes into the tBLM at ~33% of

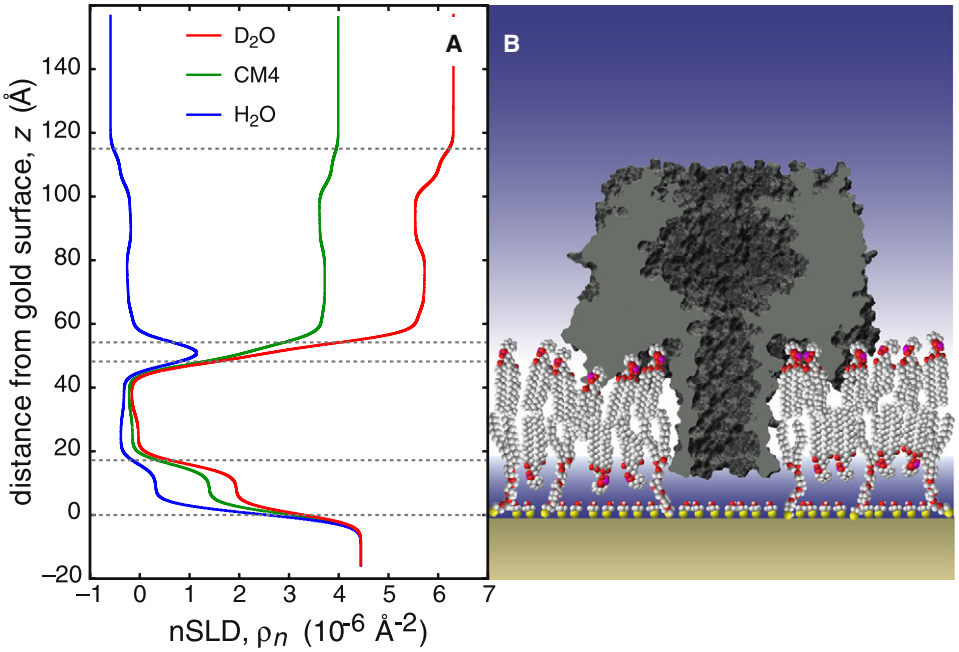

FIGURE 4 Supramolecular model of the tBLM reconstituted with α-HL. Simultaneous fitting of a molecular model to five NR data sets (two for the tBLM and three for the protein-reconstituted tBLM) leads to five nSLD profiles that are all consistent with one supramolecular structure. (*A*) The three profiles for the tBLM reconstituted with α-HL. These profiles contain the calculated contribution of the α-HL x-ray crystal structure (21) at a lateral density and insertion depth derived from the model fit. (*B*) A scaled cartoon of the system.

the maximum hexagonal packing density, as set by the dimensions of the cap domain (25). The incorporation of such a large amount of protein without bilayer collapse is another indicator of the tBLM's robustness.

In H_2O, a region of high nSLD around $z = 52$ Å (Fig. 4 *A*) provides the location of the outer membrane headgroup layer. Incorporation of α-HL leads to a significant nSLD increase in this region, indicating a strong dehydration of the headgroups. The loss of hydration expected from the compression of the lipid bilayer by the α-HL stem would be on the order of 3%, based on the observed lateral density of the cap domain near the membrane and the protein geometry. NR shows that the α-HL channel removes most of the water from the lipid headgroups (Fig. 5 *B*). This suggests that the protein cap interacts strongly with lipid headgroups and significantly perturbs their conformations, consistent with predictions based on the crystal structure (25). The overhang between the membrane-penetrating stem segment and the

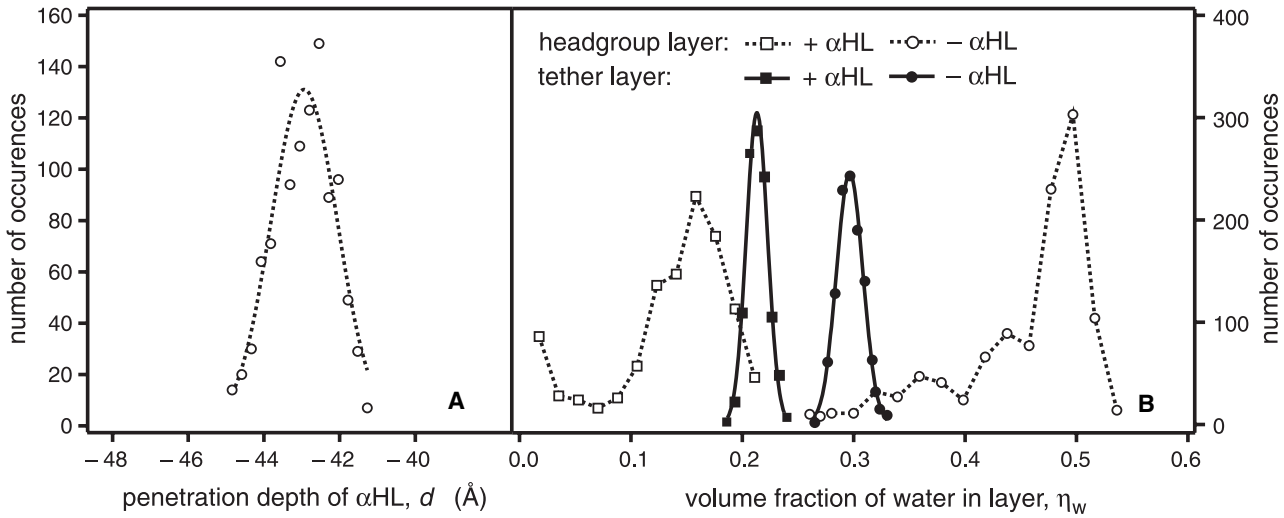

FIGURE 5 Parameter estimation and confidence limits for the supramolecular structure of α-HL reconstituted into a tBLM, determined with NR and quantified by Monte Carlo resampling (Supporting Material). Five individual data sets were linked in a composition-space modeling approach (23) that took advantage of the known α-HL crystal structure (21). Histograms of parameters describing the resampled data indicate that the protein can be localized along the surface normal with a precision of ± 1.1 Å within the fluid bilayer (*A*). (*B*) Both the lipid headgroups of the outer membrane leaflet (*open symbols; dashed lines*) and the content of the submembrane layer (*solid symbols*), including the membrane anchor and lipid headgroups of the inner leaflet, are significantly dehydrated upon reconstitution of α-HL. Parameter distributions for the submembrane layer hydration and protein insertion depth were approximately Gaussian (*fitted lines*). In contrast, the parameter distributions for the hydration of the outer lipid headgroup layer show extended tails and were evaluated by their mean values and standard deviations (for the full parameter set, see Table S3 in the Supporting Material).

cap domain is lined with hydrophilic residues that may form a suitable environment for zwitterionic phospholipid headgroups. Moreover, the edge of the cap contains hydrophobic residues that may interact with the acyl chains of the lipid bilayer. These results should aid Poisson-Nernst-Planck modeling of these systems because dehydration of the cleft between the cap domain and membrane will influence the dielectric properties of the channel-membrane system and could affect the channel conductance (32).

CONCLUSIONS

Although crystallography remains the technique of choice for determining protein structures with full atomic detail, a great deal of complementary information can be elucidated from disordered structures with other techniques, such as neutron reflectometry. Inspired by earlier work (7,18), we developed what to our knowledge is a new methodology for structural measurements on transmembrane proteins, verification of their functionality, and probing of their interactions with disordered membranes. The α-HL protein ion channel was chosen as a model system for proof-of-concept because its structure is known to high resolution (25). The technology we describe here will permit a broad range of biomedical investigations where the interaction of proteins with membranes is of immediate interest, such as studies into toxicology (33,34), Alzheimer's disease (35), cell signaling involving lipids (36), or laminopathies (37).

Although the data interpretation described here utilized a known crystal structure, the techniques developed in this work can be readily extended to the use of other structural motifs as a basis. For instance, NR-derived structures of proteins with established functionality in a tBLM could be used in conjunction with computer models to discriminate between disparate solutions in the modeling. We anticipate that this technology will complement existing methods for both structure and functional measurements of membrane proteins.

SUPPORTING MATERIAL

More explanations and descriptions, figures, tables, and references are available at http://www.biophysj.org/biophysj/supplemental/S0006-3495(08)03231-1.

Support by the National Institute of Standards and Technology (U.S. Department of Commerce) in providing the neutron research facilities used in this work is gratefully acknowledged. We thank Dr. Hirsh Nanda for helpful discussions, Rima Budvytyte for assistance with EIS experiments, and Dr. Paul A. Kienzle for support in the NR data analysis.

This work was supported by the National Science Foundation (CBET-0555201 and 0457148), the National Institutes of Health (1 RO1 RR14182 and 1 P01 AG032131-01), the American Health Assistance Foundation (A2008-307), the Lithuanian State Science and Studies Foundation (T-31/07), a National Institute of Standards and Technology-NRC Research Associateship to J.W.F.R., the National Institute of Standards and Technology Single Molecule Manipulation and Measurement Program, and the National Institute of Standards and Technology Office of Law Enforcement Standards.

Certain commercial materials, instruments, and equipment are identified in this manuscript to specify the experimental procedure as completely as possible. In no case does such identification imply a recommendation or endorsement by the National Institute of Standards and Technology, nor does it imply that the materials, instruments, or equipment identified is necessarily the best available for the purpose.

REFERENCES

1. Henderson, R., and P. N. T. Unwin. 1975. Three-dimensional model of purple membrane obtained by electron microscopy. *Nature*. 257:28–31.
2. Deisenhofer, J., O. Epp, K. Miki, R. Huber, and H. Michel. 1985. Structure of the protein subunits in the photosynthetic reaction center of Rhodopseudomonas viridis at 3 Å resolution. *Nature*. 318:618–624.
3. White, S. H. 2004. The progress of membrane protein structure determination. *Protein Sci.* 13:1948–1949.
4. Lewis, B. A., G. S. Harbison, J. Herzfeld, and R. G. Griffin. 1985. NMR structural analysis of a membrane protein – Bacteriorhodopsin peptide backbone orientation and motion. *Biochemistry*. 24:4671–4679.
5. Liang, B., and L. K. Tamm. 2007. Structure of outer membrane protein G by solution NMR spectroscopy. *Proc. Natl. Acad. Sci. USA*. 104:16140–16145.
6. Raguse, B., V. L. B. Braach-Maksvytis, B. A. Cornell, L. B. King, P. D. J. Osman, et al. 1998. Tethered lipid bilayer membranes: Formation and ionic reservoir characterization. *Langmuir*. 14:648–659.
7. Tanaka, M., and E. Sackmann. 2005. Polymer-supported membranes as models of the cell surface. *Nature*. 437:656–663.
8. McGillivray, D. J., G. Valincius, D. J. Vanderah, W. Febo-Ayala, J. T. Woodward, et al. 2007. Molecular-scale structural and functional characterization of sparsely tethered bilayer lipid membranes. *Biointerphases*. 2:21–33.
9. Schiller, S. M., R. Naumann, K. Lovejoy, H. Kunz, and W. Knoll. 2003. Archaea analogue thiolipids for tethered bilayer lipid membranes on ultrasmooth gold surfaces. *Angew. Chem. Int. Ed. Engl*. 42:208–211.
10. Vockenroth, I. K., P. P. Atanasova, A. T. A. Jenkins, and I. Köper. 2008. Incorporation of α-hemolysin in different tethered bilayer lipid membrane architectures. *Langmuir*. 24:496–502.
11. Vockenroth, I. K., C. Ohm, J. W. F. Robertson, D. J. McGillivray, M. Lösche, et al. 2008. Stable insulating tethered bilayer membranes. *Biointerphases*. 3:FA68–FA73.
12. Dura, J. A., D. Pierce, C. F. Majkrzak, N. Maliszewskyj, D. J. McGillivray, et al. 2006. AND/R: a neutron diffractometer/reflectometer for investigation of thin films and multilayers for the life sciences. *Rev. Sci. Instrum*. 77:074301.
13. Menestrina, G. 1986. Ionic channels formed by Staphylococcus aureus α-toxin. Voltage-dependent inhibition by divalent and trivalent cations. *J. Membr. Biol*. 90:177–190.
14. Glazier, S. A., D. J. Vanderah, A. L. Plant, H. Bayley, G. Valincius, et al. 2000. Reconstitution of the pore-forming toxin a-hemolysin in phospholipid/18-octadecyl-1-thiahexa(ethylene oxide) and phospholipid/*n*-octadecanethiol supported bilayer membranes. *Langmuir*. 16:10428–10435.
15. Sackmann, E. 1996. Supported membranes - scientific and practical applications. *Science*. 271:43–48.
16. Montal, M., and P. Mueller. 1972. Formation of bimolecular membranes from lipid monolayers and a study of their electrical properties. *Proc. Natl. Acad. Sci. USA*. 69:3561–3566.
17. Bezrukov, S. M., and J. J. Kasianowicz. 1993. Current noise reveals protonation kinetics and number of ionizable sites in an open protein ion channel. *Phys. Rev. Lett*. 70:2352–2355.
18. Cornell, B. A., V. L. B. Braach-Maksvytis, L. B. King, P. D. J. Osman, B. Raguse, et al. 1997. A biosensor that uses ion-channel switches. *Nature*. 387:580–583.
19. Valincius, G., D. J. McGillivray, W. Febo-Ayala, D. J. Vanderah, J. J. Kasianowicz, et al. 2006. Enzyme activity to augment the

characterization of tethered bilayer membranes. *J. Phys. Chem. B*. 110:10213–10216.

20. Als-Nielsen, J., and K. Kjaer. 1989. X-ray reflectivity and diffraction studies of liquid surfaces and surfactant monolayers. *In* Phase Transitions in Soft Condensed Matter. T. Riste and D. Sherrington, editors. Plenum Press. New York. 113–138.
21. Kienzle, P. A., M. Doucet, D. J. McGillivray, K. V. O'Donovan, N. F. Berk, et al. 2000–2009. ga_refl. http://www.ncnr.nist.gov/reflpak/garefl.html.
22. Parratt, L. G. 1954. Surface studies of solids by total reflection of x-rays. *Phys. Rev*. 95:359–369.
23. Vaknin, D., K. Kjaer, J. Als-Nielsen, and M. Lösche. 1991. Structural properties of phosphatidylcholine in a monolayer at the air/water interface. Neutron reflection study and reexamination of x-ray reflection experiments. *Biophys. J*. 59:1325–1332.
24. Wiener, M. C., and S. H. White. 1991. Fluid bilayer structure determination by the combined use of x-ray and neutron diffraction. II. "Composition-space" refinement method. *Biophys. J*. 59:174–185.
25. Song, L., M. R. Hobaugh, C. Shustak, S. Cheley, H. Bayley, et al. 1996. Structure of staphylococcal α-hemolysin, a heptameric transmembrane pore. *Science*. 274:1859–1865.
26. Connolly, M. L. 1983. Analytical molecular-surface calculation. *Appl. Crystallogr*. 16:548–558.
27. Raistrick, I. D., D. R. Franceschetti, and J. R. Macdonald. 2005. Theory. *In* Impedance Spectroscopy: Theory, Experiment, and Applications. 2nd ed. E. Barsoukov and J. R. Macdonald, editors. Wiley. New York, 27–117.
28. Redwood, W. R., F. R. Pfeiffer, J. A. Weisbach, and T. E. Thompson. 1971. Physical properties of bilayer membranes formed from a synthetic saturated phospholipid in decane. *Biochim. Biophys. Acta*. 233:1–6.
29. Dilger, J. P., S. G. A. McLaughlin, T. J. McIntosh, and S. A. Simon. 1979. Dielectric constant of phospholipid bilayers and the permeability of membranes to ions. *Science*. 206:1196–1198.
30. Bezrukov, S. M., I. Vodyanoy, R. A. Brutyan, and J. J. Kasianowicz. 1996. Dynamics and free energy of polymers partitioning into a nanoscale pore. *Macromolecules*. 29:8517–8522.
31. Majkrzak, C. F., N. F. Berk, S. Krueger, J. A. Dura, M. Tarek, et al. 2000. First-principles determination of hybrid bilayer membrane structure by phase-sensitive neutron reflectometry. *Biophys. J*. 79:3330–3340.
32. Coalson, R. D., and M. G. Kurnikova. 2005. Poisson-Nernst-Planck theory approach to the calculation of current through biological ion channels. *IEEE Trans. Nanobioscience*. 4:81–93.
33. Halverson, K., R. G. Panchal, T. L. Nguyen, R. Gussio, S. F. Little, et al. 2005. Anthrax biosensor, protective antigen ion channel asymmetric blockade. *J. Biol. Chem*. 280:30056–30062.
34. Kent, M. S., H. Yim, J. K. Murton, S. Satija, J. Majewski, et al. 2008. Oligomerization of membrane-bound diphtheria toxin (CRM197) facilitates a transition to the open form and deep insertion. *Biophys. J*. 94:2115–2127.
35. Valincius, G., F. Heinrich, R. Budvytyte, D. J. Vanderah, Y. Sokolov, et al. 2008. Soluble amyloid oligomers affect dielectric membrane properties by bilayer insertion and domain formation: Implications for cell toxicity. *Biophys. J*. 95:4845–4861.
36. Wymann, M. P., and R. Schneiter. 2008. Lipid signalling in disease. *Nat. Rev. Mol. Cell Biol*. 9:162–176.
37. Liu, B., and Z. Zhou. 2008. Lamin A/C, laminopathies and premature ageing. *Histol. Histopathol*. 23:747–763.

submitted to *Biophys. J.* August-12, 2008
revised version: October-31, 2008

SUPPLEMENTARY MATERIAL:

Structure of functional *Staphylococcus aureus* α-hemolysin channels in tethered bilayer lipid membranes

Duncan J. McGillivray,[1,2,§,‡] Gintaras Valincius,[3,‡] Frank Heinrich,[1,2] Joseph W. F. Robertson,[4] David J. Vanderah,[5] Wilma Febo-Ayala,[5,§§] Ilja Ignatjev,[3] Mathias Lösche[1,2,*] and John J. Kasianowicz[4]

1. National Institute of Standards and Technology (NIST) Center for Neutron Research (NCNR), Gaithersburg, Maryland 20899-6102
2. Physics Department, Carnegie Mellon University, Pittsburgh, Pennsylvania 15213-3890
3. Institute of Biochemistry, Mokslininku 12, LT-2600 Vilnius, Lithuania
4. Semiconductor Electronics Division, NIST, Electronics and Electrical Engineering Laboratory, Gaithersburg, Maryland 20899-8120
5. Biochemical Sciences Division, NIST, Chemical Sciences and Technology Laboratory, Gaithersburg, Maryland 20899-8313

This file describes the impedance spectroscopy data modeling and provides EIS results on αHL-reconstituted tBLMs in buffer (section I) and in PEG solutions (section II), and provides a full description of the neutron reflection data, models and scattering length density profiles (section III). It gives a determination of parameter confidence limits by a *Monte Carlo* resampling method (section IV) and describes auxiliary experiments with tBLMs using a longer tether (section V) that complement the results described in the main paper.

*Correspondence:

Mathias Lösche,
Physics Department, Carnegie Mellon University, 5000 Forbes Ave., Pittsburgh, PA 15213-3890
412-268-2735, fax: 412-268-8252, emb: quench@cmu.edu

I. Modeling of electrochemical impedance spectra

To accurately determine area-normalized electronic components from EIS data, the roughness factor of each electrode was measured by two independent electrochemical techniques: capacitance ratio and gold oxide stripping coulometry (1) prior to the experiment, and determined as 1.39 ± 0.04. EIS data were fitted to the models in Scheme S1 using *Zview 2.9* (Scribner Associates, Inc., Southern Pines, NC), using data-modulus weighting. Model A, an equivalent circuit model (ECM) we recently developed, describes the properties of tBLMs particularly well (2-4). It accounts for the bilayer capacitance and the Helmholtz capacitance of an interface between the gold and the electrolyte (CPE_{tBLM}); a conduction pathway parallel to CPE_{tBLM} consists of CPE_{pores} and R_{pores} and accounts for the conductance of either defects or αHL-induced pores. tBLM systems with a small defect density exhibit CPE_{pores} exponent values close to α = 0.5, while an increasing density of the ion-conducting αHL pores shifts this parameter towards α = 1. CPE_{pores} is determined by the Helmholtz capacitance and the specific conductance and thickness of the electrolyte reservoir confined between the electrode and the phospholipid bilayer. R_{pores} corresponds to the resistance of the pores. Cole-Cole plots of electrochemical impedance spectra of an tBLM before and after αHL incubation, fitted to model A, are shown in Fig. S1.

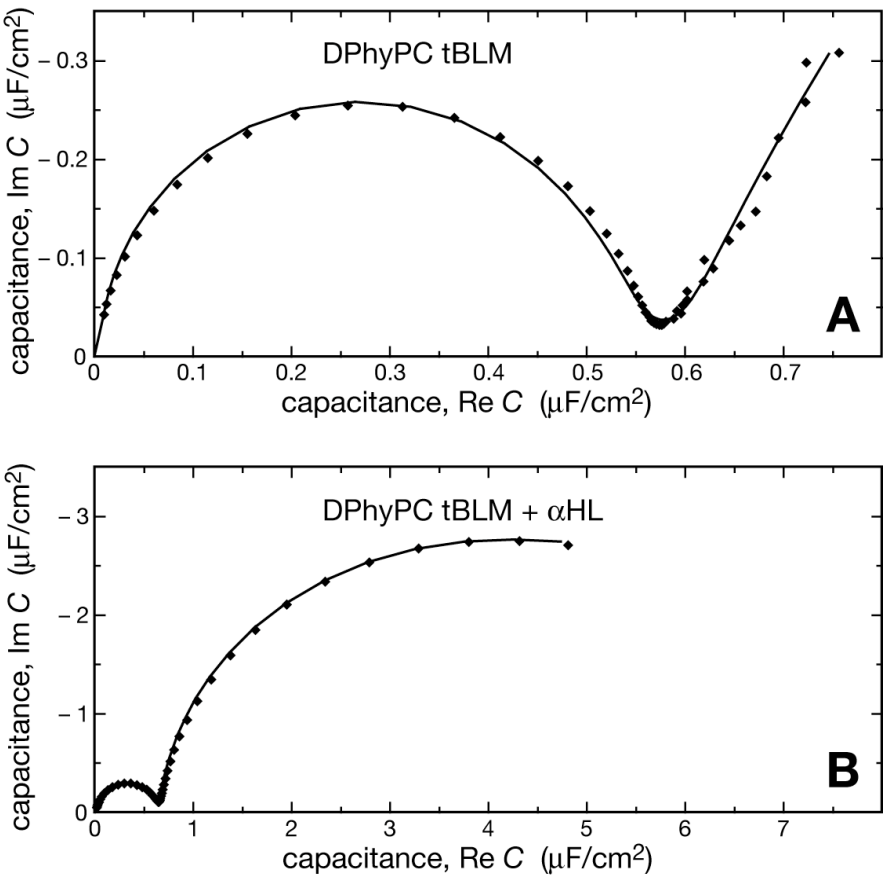

Figure S1: Cole-Cole plots of a DPhyPC tBLM before (A) and after (B) αHL reconstitution. (A) The tBLM was formed on a SAM prepared from a 30:70 (mol:mol) solution of WC14 and βME. The electrolyte was 0.1 M NaCl, 0.01 M Na-phosphate buffer at pH 7.5. Frequency range is from 1 to 65,000 Hz. (B) tBLM spectrum after incubation for 113 min with a 152 nM solution of αHL. Frequency range is from 1 to 39,800 Hz. All data are normalized with respect to the surface area. The solid lines show fits to ECM A of Scheme S1.

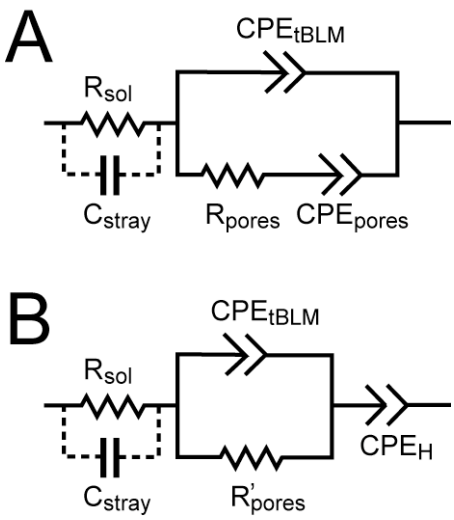

Scheme S1: Equivalent circuit models of the tBLM in solution. Two alternate models, A and B, were considered. The CPEs are constant phase elements, whose impedances are defined as $Z_{CPE} = 1/CPE \times 1/(i\omega)^{\alpha}$, where CPE is the coefficient of the element. $\omega = 2\pi f$, with f the frequency in Hz. α is the CPE exponent. R_{sol} is the solution resistance, and C_{stray} accounts for the capacitance associated of cables, connectors and the electrochemical cell. Model A attributes a constant phase element CPE_{pores} to the pores in the membrane whereas model B assumes a CPE_H for the Helmholtz layer.

EI spectra fitted with ECM A yielded fit qualities of (typically) $\chi^2 < 2\times10^{-4}$. Results are summarized in Table S1. Incubation with αHL solution increases CPE_{tBLM} as well as CPE_{pores} and α_{pores}. However, the most dramatic change occurs in R_{pores}, which exhibits a ca. 30-fold decrease upon incubation with protein solution, which we attribute to the αHL-induced conductance, $Y_{pores} = R_{pores}^{-1}$, of the membrane.

We considered other ECMs for the tethered membranes (***e.g.***, ECM B in Scheme S1). These did not fit the experimental data well compared to ECM A. Under certain conditions, the two models, A and B, may be degenerate, which may lead to a different interpretation of the electrochemical properties of the interface. Specifically, the exponent of CPE_{pores} increased from $\alpha_{pores} \approx 0.5$ to $\alpha_{pores} \rightarrow \alpha_{tBLM}$ upon incubation with αHL (see Table S1). At $\alpha_{pores} = \alpha_{tBLM}$, model A becomes degenerate with model B. Upon incubation with αHL, the exponent of CPE_{pores} increased from $\alpha_{pores} \approx 0.5$ to $\alpha_{pores} \rightarrow \alpha_{tBLM} \approx 0.98$ (Table S1). In the degenerate case, the pore conductance described as R_{pores} in series with CPE_{pores} parallel to the insulating membrane is replaced by (5)

$$R'_{pores} = R_{pores} \cdot \left(\frac{CPE_{pores}}{CPE_{pores} + CPE_{tBLM}} \right)^2 \qquad (1)$$

Because $R'_{pores} < R_{pores}$, the αHL-induced conductance across the membrane is greater in ECM B than in ECM A. Although α_{pores} is not strictly equal to α_{tBLM}, the uncertainty in α limits our ability to distinguish between the two models. A best-fit parameter set is included in Table S1 for comparison with the best fit using ECM A. In this case, χ^2 must be tested for both models. Indeed, the χ^2 for model A is about 10-fold smaller than that for model B. Moreover, while R_{pores} is less in model B than in model A, it is also significantly less than predicted by Eqn. (1), which is physically unrealistic. This rules out the possibility of degeneracy and justifies the validity of model A.

Table S1: Model parameters for the DPhyPC tBLM EIS spectra shown in Fig. S1 derived from a single sample. Data is normalized with respect to the real surface area. Normalization of R_{sol} and C_{stray} keeps the whole data set consistent.

parameter \ system	tBLM before αHL reconstitution (model A)	tBLM after αHL reconstitution (model A)	tBLM after αHL reconstitution (model B)
CPE_{tBLM}, $\mu F \cdot cm^{-2} \times s^{(\alpha-1)}$	0.696 ± 0.007	0.791 ± 0.003	0.908 ± 0.016
α_{tBLM}	0.975 ± 0.001	0.9741 ± 0.0004	0.992 ± 0.004
CPE_{pores}, $\mu F \cdot cm^{-2} \times s^{(\alpha-1)}$	1.575 ± 0.119	7.38 ± 0.04	
α_{pores}	0.51 ± 0.10	0.86 ± 0.04	
CPE_{H}, $\mu F \cdot cm^{-2} \times s^{(\alpha-1)}$			7.87 ± 0.12
α_{H}			0.87 ± 0.01
R_{pores}, $k\Omega \cdot cm^2$	305 ± 15	12.25 ± 0.04	8.80 ± 0.15
R_{sol}, $\Omega \cdot cm^2$	53.8 ± 0.2	65.4 ± 0.1	64.3 ± 0.3
C_{stray}, $nF \cdot cm^{-2}$	6.14 ± 0.35	7.99 ± 0.16	7.06 ± 0.51
χ^2	$15.1 \cdot 10^{-5}$	$1.52 \cdot 10^{-5}$	$14.6 \cdot 10^{-5}$

II. EIS of protein-reconstituted tBLMs in PEG solutions

Upon introduction of differently-sized PEGs (15% w/w), reversible changes in the EIS data were observed in the frequency range that is mostly determined by R_{pores}, as the modeling shows. In particular PEGs with a mean molecular mass < 2,250 g/mol increased $|Z|$ and shifted the minimum in ϕ towards lower frequencies (Fig. S2), while PEGs with a mean molecular mass > 2,250 g/mol caused the opposite effects. Representative fits to the model obtained on one single tBLM are listed in Table S2. The PEGs affect mainly R_{pores}, which changes by ≈ –35% (PEG200) to ≈ +15% (PEG3400) from its value in PEG-free buffer. Other parameters were less affected by the polymer, except for CPE_{pores}, which changed by –10% in PEG200, presumably due to penetration of polymer molecules into the submembrane space.

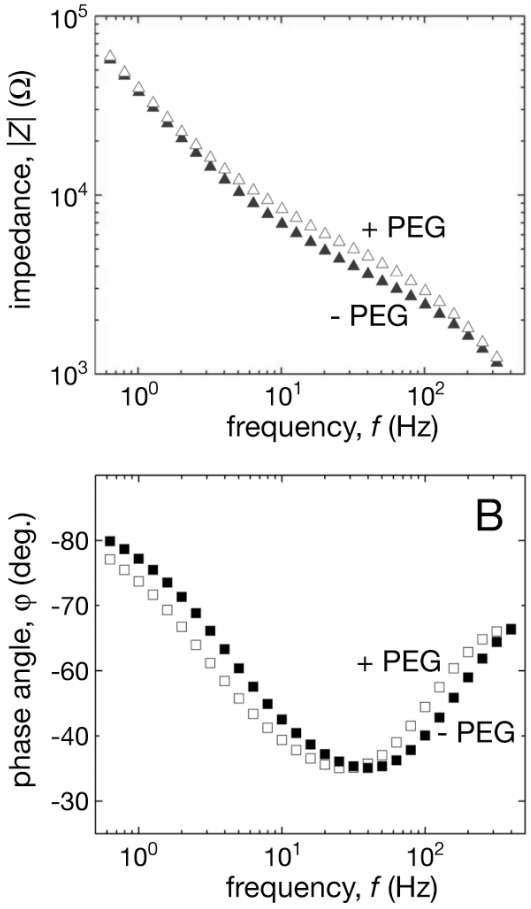

Figure S2: Effect of 15% (w:w) 400 g/mol PEG on the impedance (Bode plots) of a tBLM containing αHL channels. Data are normalized with respect to the surface area.

Table S2: Model parameters for tBLMs in solutions without and with differently-sized PEG.[a,b,c]

parameter	no PEG	15% w/w PEG200 (relative changes)	15% w/w PEG3400 (relative changes)
CPE_{tBLM}, μF · cm^{-2}×s$^{(α-1)}$	0.793	0.818 (+3%)	0.862 (+8%)
$α_{tBLM}$	0.974	0.969 (–1%)	0.963 (–1%)
CPE_{pores}, μF · cm^{-2}×s$^{(α-1)}$	4.04	3.64 (–10%)	4.11 (+2%)
$α_{pores}$	0.844	0.856 (+1%)	0.846 (+0%)
$Y_{pores} = R_{pores}^{-1}$, μS · cm^{-2}	638	414 (–35%)	717 (+12%)
$χ^2$	$8.1 \cdot 10^{-5}$	$9.3 \cdot 10^{-5}$	$8.2 \cdot 10^{-5}$

[a]The buffer was 0.1 M NaCl, 0.01 M Na-phosphate at pH 7.5.
[b]The tBLM was incubated for ca. 1 h with 50 nM αHL solution in a similar buffer at pH 4.5. The incubation solution was then replaced with buffer (pH 7.5) that was free of αHL.
[c]Numbers in parentheses indicate changes of a particular parameter with respect to its value in a PEG-free solution. Relative fitting errors were below 1% for all listed parameters.

III. Neutron reflection

αHL reconstituted into WC14-based tBLMs. Figure S3 shows the full range of experiments with isotopically distinct bulk solvents performed before and after the incorporation of αHL into the membrane. Addition of αHL into the membrane resulted in subtle, yet significant changes in the NR spectra, particularly at low momentum transfer Q_z.

These data were fitted using a slab model with layers of uniform neutron scattering length density (nSLD) for each of the chemically distinct components of the interface: Si, SiO_x, Cr, Au, OEG tether, inner bilayer leaflet, outer bilayer leaflet, headgroups, and solvent. In the composition-space refinement evaluation (6,7) of the neutron reflection data, nSLDs in slabs representing the tBLM and αHL (z = 0 – 120 Å in Fig. S4) was parameterized in terms of volume fractions, η, of organic material and solvent (8), subject to the constraint $\sum \eta_j = 1$, i.e. volume not occupied by organic material is filled by aqueous buffer of the appropriate isotopic composition. For example, the hydration of a lipid headgroup (hg) layer is the composite result of three NR spectra measured with different neutron contrasts:

$$\eta_{water} = \frac{n_w \cdot V_w}{n_w \cdot V_w + V_{hg}} = \frac{V_w\left(\rho^w V_{hg} - b_{hg}\right)}{V_w\left(\rho^w V_{hg} - b_{hg}\right) - V_{hg}\left(\rho^w V_w - b_w\right)} \qquad (2)$$

where n_w is the (fractional) number of waters per lipid hg, V is a molecular volume [V_w = 10 Å^3 for water, indiscriminate of isotopic composition, V_{hg} = 200 Å^3, see (9)] and b is neutron scattering length. The subscript w (= D_2O, CM4, H_2O) indicates the isotopic composition of water and ρ is the experimentally determined nSLD, measured in the system under three distinct isotopic buffer compositions specified by the superscript. Similar relations hold for the alkane region, where the monolayer proximal to the solid support is frequently slightly incomplete and incorporates water-filled defects amounting to typically 5% of its overall area.

It has been determined from grazing-incidence x-ray diffraction studies of a large number of amphiphiles in Langmuir monolayers (10) that the alkane density in lipid membranes cannot exceed 1 alkane chain per 19.5 Å^2. For the evaluation of NR data, this confines the nSLD of the alkane phase to be $\rho > -0.5\times10^{-6}$ Å^{-2}. While restricting the phytyl nSLD to fall above this lower limit in the model, we observed that the best-fit parameters in histograms derived from a novel Monte-Carlo resampling procedure (details, see section IV.) for ρ_{phytyl} peaked at this limit. Consequently, we denoted this parameter as “fixed” at this value (Table S3). This best-fit model suggests an unphysically high phytyl chain density. However, the deviation of this result from the expected value, $\rho_{phytyl} \approx -0.3\times10^{-6}$ Å^{-2} (11,12), equals the typical measurement uncertainty of this parameter. In fact, we occasionally observed a similar overestimation of non-deuterated al-

kane chain density for various non-deuterated lipids when using box models for data analysis. We assume that this is due to intrinsic weaknesses of the box model in describing the interface between phospholipid headgroups and alkyl chains, studied extensively in earlier work on Langmuir monolayers (13). While we were able to resolve this flaw of the box model in developing more complex phospholipid models for Langmuir monolayers (14), we note that the application of an adequately complex model for bilayer lipids is currently beyond the scope of or modeling capabilities of tBLMs, and may exceed the information content of the obtained reflectivity data. We thoroughly verified that variations in the model using fixed values for ρ_{phytyl} between –0.5 and $–0.3\times10^{-6}$ $Å^{-2}$ did not significantly alter the structural impact of αHL incorporation on the bilayer and are therefore confident that our conclusions in the paper are not affected by this result.

The αHL spans several layers in the model; the contribution of the protein to the nSLD of these layers was calculated from the published crystal structure (15). For convenience in the model evaluation, the in-plane protein density $\sigma_{αHL}$ in/at the membrane was parameterized in terms of a square lattice of protein caps in the layer adjacent to the tBLM, assuming that the diameter of the cap sets the limit for dense packing. The evaluation of this parameter is reported in Fig. S5A (green plot symbols). In distinction, the protein density reported in Table S3 was converted assuming a hexagonal lattice parameter according to the relation:

$$\sigma_{\alpha HL}^{hex} = \sqrt{3}/2 \times \sigma_{\alpha HL}^{square}.$$

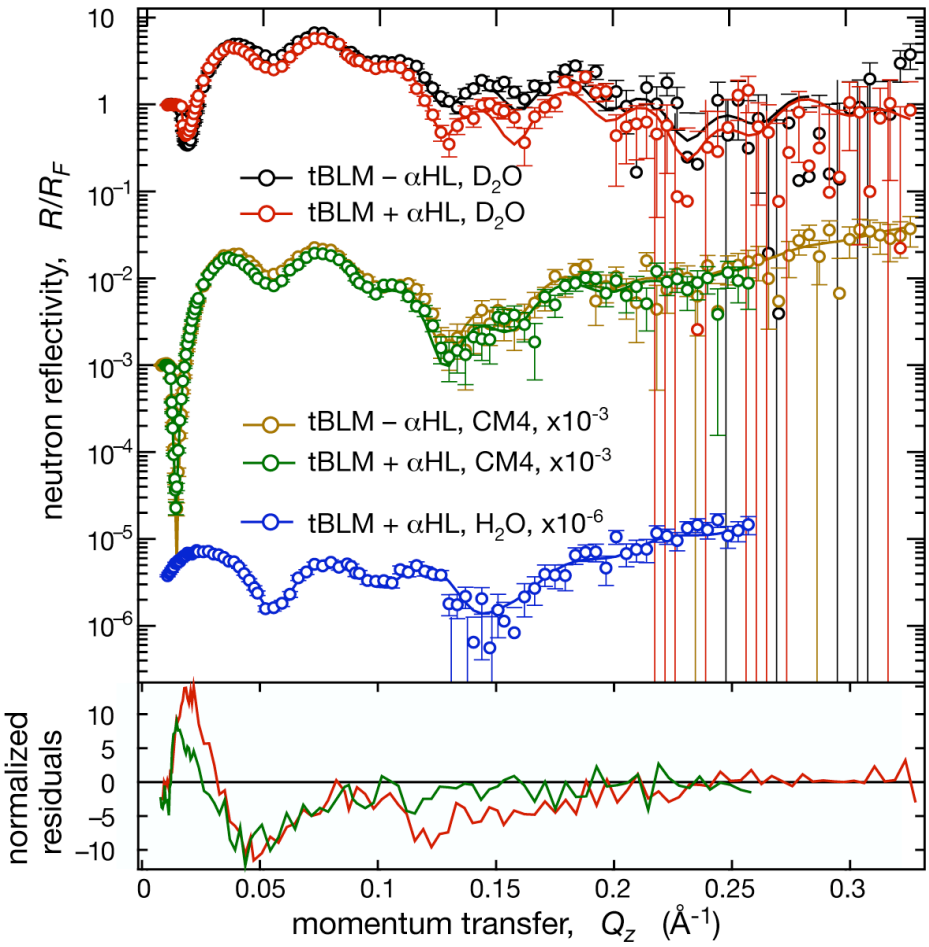

Figure S3: Comprehensive NR data. Main panel: Fresnel-normalized NR reflection data sets obtained from one tBLM (WC14:βME = 30:70, completed with DPhyPC) before and after reconstitution of αHL channel proteins at various solvent contrasts. The upper pair of data sets are identical with those in Fig. 3 in the paper. Lower panel: Error-weighted residuals between data with αHL and without αHL. The red line (D_2O data sets) is the same as in Fig. 3. The green line is for the CM4 data sets. Solid lines in the main panel are the reflectivities computed from the nSLD profiles shown in Fig. S4.

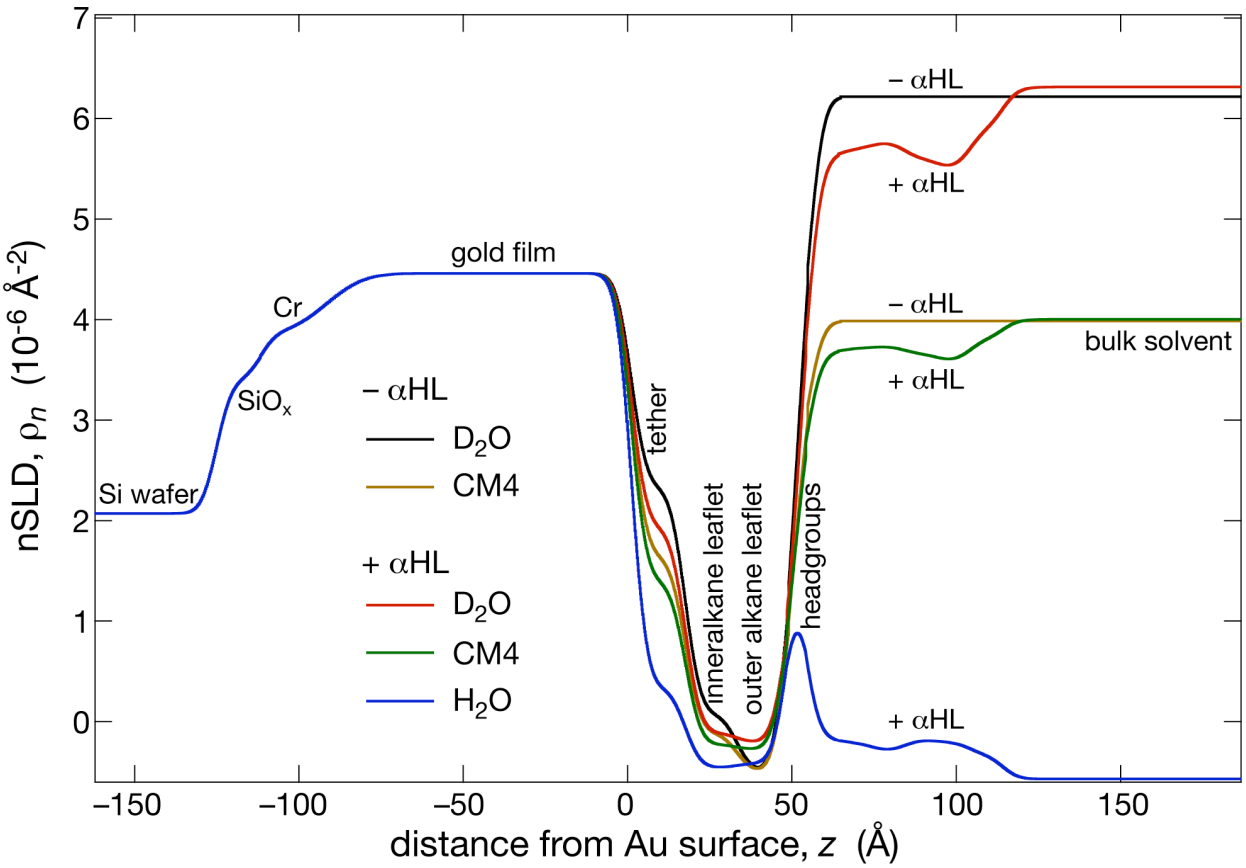

Figure S4: Neutron scattering length density profiles derived from a simultaneous model fit to all data shown in Fig. S3. The color code is consistent with that of the data sets. Details are presented in Table S3.

Table S3: Model parameters derived from a simultaneous fit to NR data at different solvent contrasts for a tBLM prepared with WC14/βME (1:3) and DPhyPC, with and without αHL.[a,b]

parameter \ data set	– αHL, D_2O buffer	– αHL, CM4	+ αHL, D_2O buffer	+ αHL, CM4	+ αHL, H_2O buffer
thickness SiO_x, Å	16.1 ± 0.9				
thickness Cr, Å	22.4 ± 1.0				
thickness Au, Å	88.0 ± 1.0				
thickness tether layer, Å	17.0 ± 0.7				
thickness inner/outer alkane layer[c], Å	15.4 ± 0.4		14.9 ± 0.4		
thickness outer headgroup layer, Å	7.6 ± 0.4		7.8 ± 0.4		
penetration depth of αHL[d], Å	n/a		–42.8 ± 1.1		
lipid nSLD, 10^{-6} Å^{-2}	–0.50 (fixed)				
nSLD bulk solvent, 10^{-6} Å^{-2}	6.22 ± 0.01	3.99 ± 0.01	6.31 ± 0.01	4.00 ± 0.01	–0.56 (fixed)
vol. fraction of water in tether layer	0.29 ± 0.02		0.21 ± 0.02		
vol. fraction of water in inner lipid leaflet[e]	0.08 ± 0.01		0.04 ± 0.01		
vol. fraction of water in outer lipid leaflet[e]	0.00 ± 0.01		0.00 ± 0.01		
vol. fraction of water in outer headgroup layer[e]	0.45 ± 0.09		0.13 ± 0.08		
in-plane αHL density[f]	n/a		33 ± 1%		
global roughness, Å	6.9 ± 1.0				
χ^2	2.13	2.52	3.45	1.79	1.14
χ^2 (global)	2.37				

[a]Parameter values printed across neighboring columns were determined by requiring that those parameters fit the data sets represented in these columns simultaneously (6,7).
[b]nSLDs were taken from tabulated values or estimated from molecular models: Si (2.07×10^{-6} Å^{-2}), SiO_x (3.4×10^{-6} Å^{-2}), Au (4.5×10^{-6} Å^{-2}), $HS(EO)_6$-glycerol tethers, βME and phosphatidylcholine headgroups within the tether layer (0.60×10^{-6} Å^{-2}), outer phosphatidylcholine headgroup layer (1.8×10^{-6} Å^{-2}).
[c]The inner and outer alkane layers were assumed to be of equal thickness.
[d]"Penetration depth of αHL" refers to the difference between the upper interface of the outer lipid headgroup layer and the lower end of the αHL stem.
[e]The remaining content of these layers is composed of lipid and protein material in a composition that derives from the amino acid composition along the protein's symmetry axis, as determined from the αHL crystal structure (15), the in-plane density of αHL and the protein's penetration depth into the bilayer.
[f]"In-plane αHL density" refers to a dense hexagonal packing of the protein caps in the layer outside of the tBLM, assuming a cap diameter, D_{cap} = 105 Å.

IV. Determination of parameter confidence limits in neutron reflection

Because the interference patterns of the NR results are dominated by the physical properties of the inorganic surface structure of the support (primarily, the gold film), it is important to show that all parameters are well determined in the composition-space refinement procedure. Thus, we determined the confidence limits of the model by *Monte Carlo* resampling of synthetic data sets (16).

In this procedure, N = 1,000 synthetic data sets were cloned from the experimental data by creating random, Gaussian-weighted deviations from the true data based on the uncertainty of each experimental data point determined by counting statistics. By coupling these simulated data sets in the same way as in the determination of the best-fit model (indicated by parameter spreading across the columns in Table S3), N slightly different best-fit parameter sets were determined. The best-fit parameter sets were binned and analyzed. In most cases, the resulting parameter distributions were well described by Gaussians. Because some distributions showed asymmetric tails, uncertainties are reported as (standard deviation $\sigma \times \sqrt{2}$), representing ca. 84% confidence limits.

Further to providing an objective measure of the parameter confidence limits, *Monte Carlo* resampling shows that the model is adequately parameterized given the quality of the experimental data, because it resulted in narrow histograms that were in most cases Gauss-shaped. If the model were overparameterized, one would expect flat histogram distributions that are not seen in the results. The *Monte Carlo* resampling also provides evidence that we obtain the global minimum within our model. If the fit were trapped in local minima, this would have produced parameter distributions with multiple peaks. However, that was not the case (see Fig. S5).

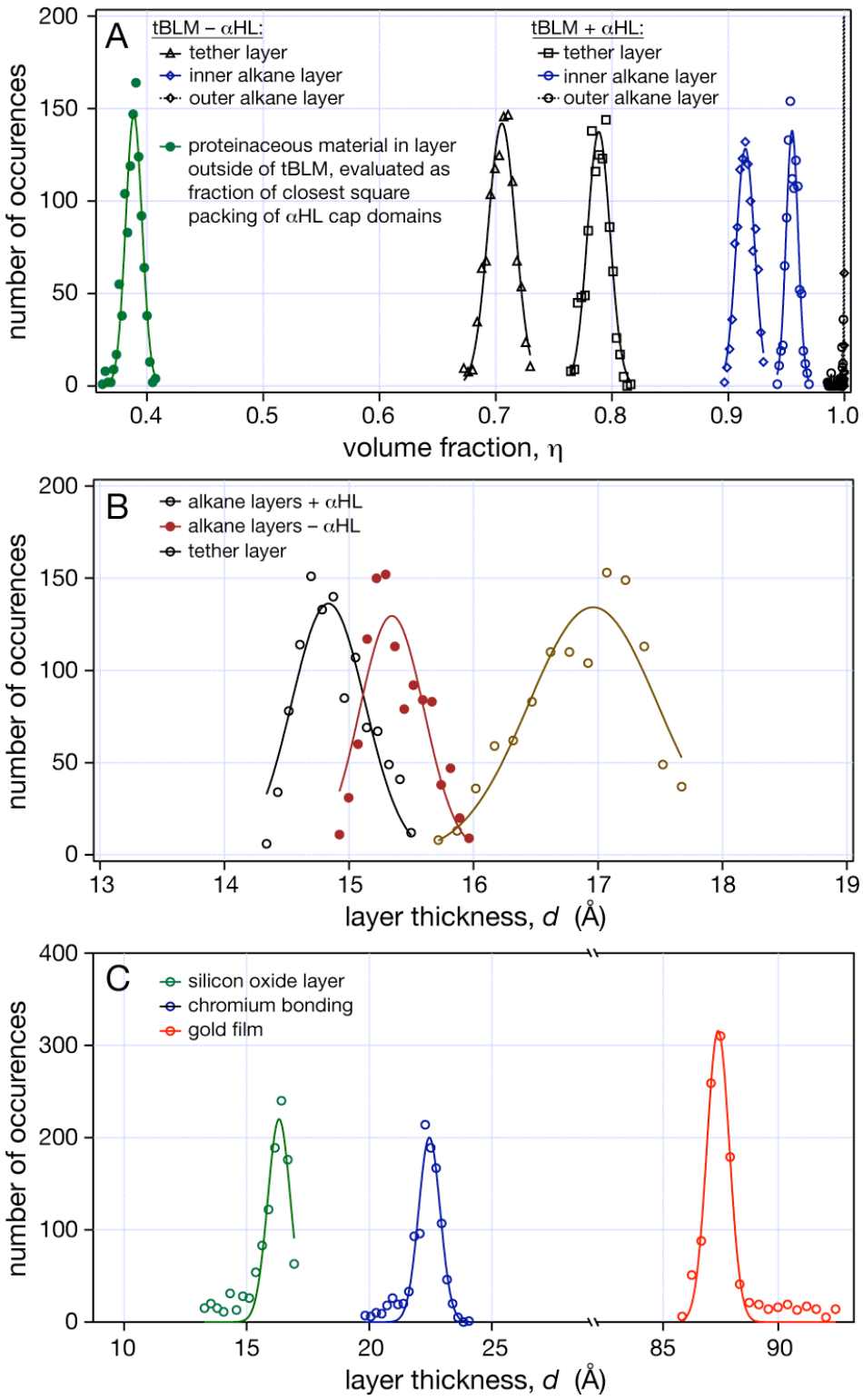

Figure S5: Results from *Monte Carlo* resampling. Parameter distribution histograms for (A) volume fraction of the organic materials, (B) geometric properties of the layers that compose the tBLM and (C) geometric properties of the inorganic substrate surface structure. Continuous lines are Gaussian fits.

V. Bilayers from PDP-PEG2000-DSPE-based bilayer surfaces

To test the effect of the proximity of the gold surface on the structural details of αHL membrane incorporation, control experiments were performed with PDP-PEG2000-DSPE-based tBLMs. Fig. S6 shows a complete solvent contrast data set collected for such a surface. Modeling was performed using the same conditions as for WC14-based tBLMs. The result in Fig. S7 shows that the PEG moiety ($n \approx 45$) increases the thickness of the space between the gold electrode and the inner membrane leaflet to ≈ 60 Å. Although these tBLMs are not electrically insulating, NR shows that the membrane covers the gold surface homogeneously and that αHL reconstitution occurs as it does in the WC14-based tBLMs. *Monte Carlo* resampling of the results in Fig. S6 suggests that the differences between the neutron reflectivities in the absence and presence of αHL are statistically significant (*not shown*). The nSLD profiles (Fig. S7) suggest that protein association with the membrane is similar in both systems. Thus, the structural organization of the reconstituted protein in the membrane does not depend on distance from the gold electrode.

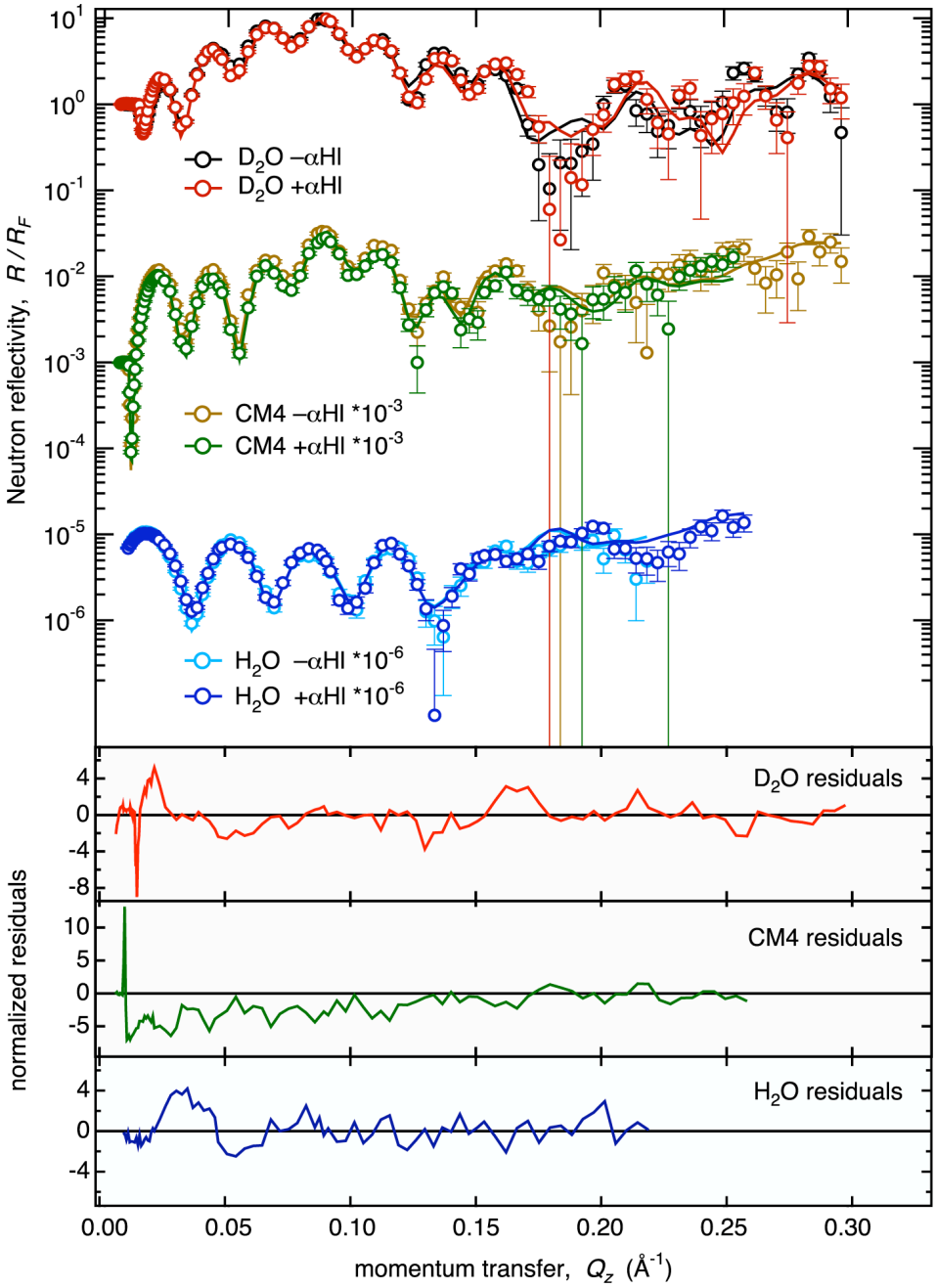

Figure S6: NR data for an alternate tBLM preparation. Main panel: Fresnel-normalized NR reflection data sets obtained from a tBLM (PDP-PEG2000-DSPE, completed with DPhyPC) before and after reconstitution of αHL channel proteins at various solvent contrasts. Lower panel: Error-weighted residuals between data with αHL and without αHL. Solid lines in the main panel are the reflectivities computed from the nSLD profiles shown in Fig. S7.

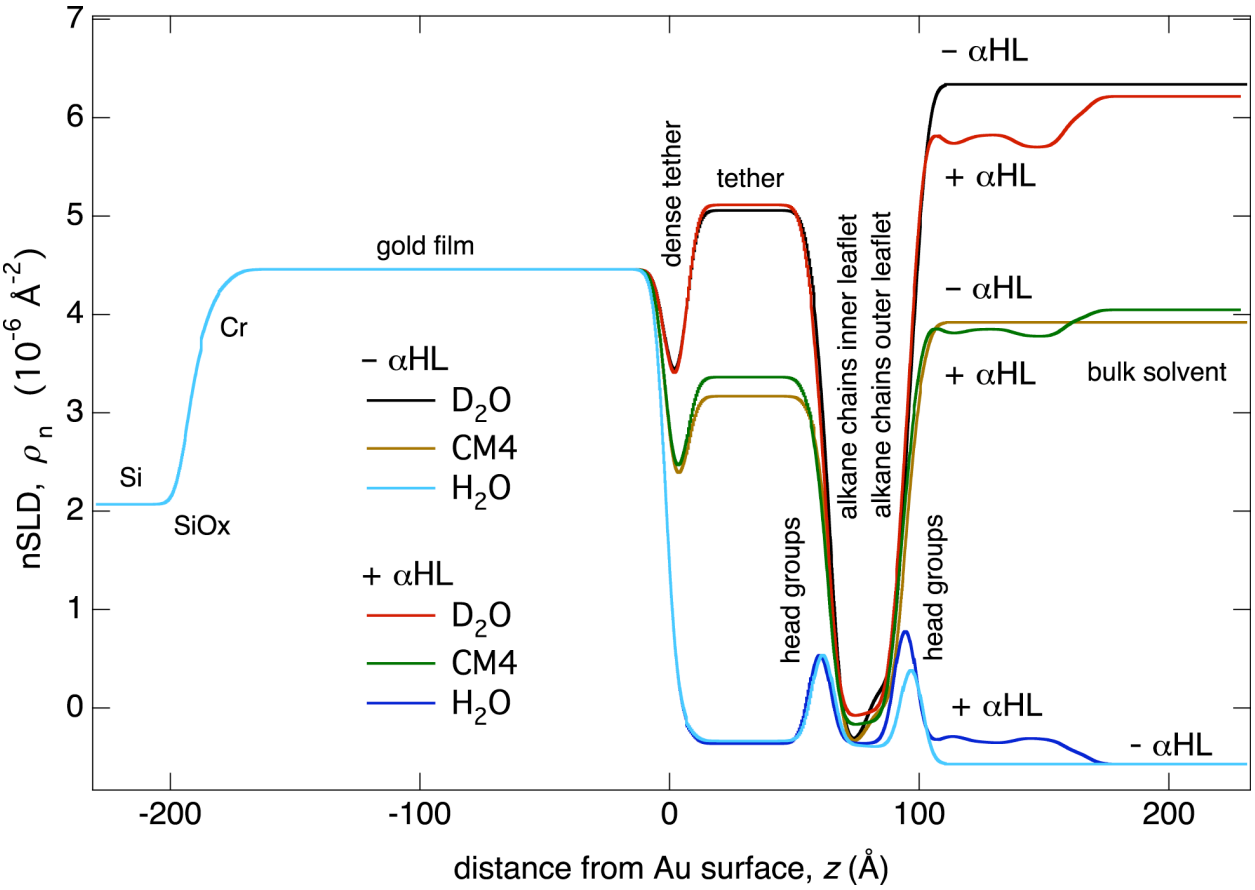

Figure S7: nSLD profiles derived from a simultaneous model fit to all data sets shown in Fig. S6. The color code is consistent with that of the data sets. Details are presented in Table S4.

Table S4: Model parameters derived from a simultaneous fit to NR data at different solvent contrasts for a tBLM prepared with PDP-PEG2000-DSPE and DPhyPC, without and with αHL.[a,b]

parameter \ data set	– αHL, D_2O buff.	– αHL, CM4	– αHL, H_2O buff.	+ αHL, D_2O buff.	+ αHL, CM4	+ αHL, H_2O buff.
thickness SiO_x, Å	6.7 ± 5.5					
thickness Cr, Å	7.2 ± 5.9					
thickness Au, Å	178.6 ± 2.4					
thickness dense tether layer, Å	8.5 ± 0.8					
thickness highly hydrated tether layer, Å	51.3 ± 0.9			49.9 ± 0.9		
thickness inner/outer alkane layer, Å	14.3 ± 0.5			13.7 ± 0.5		
thickness headgroup layers, Å	7.0 (fixed)					
penetration depth of αHL, Å	n/a			–35.8 ± 9.0		
lipid nSLD, 10^{-6} Å^{-2}	–0.40 (fixed)					
nSLD bulk solvent, 10^{-6} Å^{-2}	6.21 ± 0.01	4.05 ± 0.01	–0.56 (fixed)	6.33 ± 0.01	3.92 ± 0.01	–0.56 (fixed)
vol. fraction of water in dense tether layer	0.44 ± 0.04					
vol. fraction of water in hydrated tether layer	0.78 ± 0.01			0.80 ± 0.01		
vol. fraction of water in inner headgroup layer	0.33 ± 0.08					
vol. fraction of water in inner lipid leaflet	0.00 ± 0.03			0.02 ± 0.03		
vol. fraction of water in outer lipid leaflet	0.09 ± 0.03			0.04 ± 0.03		
vol. fraction of water in outer headgroup layer	0.41 ± 0.10			0.17 ± 0.09		
in-plane αHL density	n/a			24 ± 2%		
global roughness, Å	8.6 ± 0.6					
χ^2	4.06	4.31	3.69	4.84	5.01	3.79
χ^2 (global)	4.55					

[a]Parameter values printed across neighboring columns were determined by requiring that those parameters fit the data sets represented in these columns simultaneously.
[b]Uncertainties were determined from the covariance matrix of a Levenberg-Marquardt least square minimization.

REFERENCES

1. Trasatti, S. and O. A. Petrii. 1991. Real surface area measurements in electrochemistry. *Pure Appl. Chem.* 63:711-734.
2. McGillivray, D. J., G. Valincius, D. J. Vanderah, W. Febo-Ayala, J. T. Woodward, F. Heinrich, J. J. Kasianowicz, and M. Lösche. 2007. Molecular-scale structural and functional characterization of sparsely tethered bilayer lipid membranes. *Biointerphases* 2:21-33.
3. Valincius, G., F. Heinrich, R. Budvytyte, D. J. Vanderah, Y. Sokolov, J. E. Hall, and M. Lösche. 2008. Soluble amyloid oligomers affect dielectric membrane properties by bilayer insertion and domain formation: Implications for cell toxicity. *Biophys. J.* 95:4845-4861.
4. Valincius, G., D. J. McGillivray, W. Febo-Ayala, D. J. Vanderah, J. J. Kasianowicz, and M. Lösche. 2006. Enzyme activity to augment the characterization of tethered bilayer membranes. *J. Phys. Chem. B* 110:10213-10216.
5. Berthier, F., J. P. Diard, and R. Michel. 2001. Distinguishability of equivalent circuits containing CPEs: Part I. Theoretical part. *J. Electroanal. Chem.* 510:1-11.
6. Vaknin, D., K. Kjaer, J. Als-Nielsen, and M. Lösche. 1991. Structural properties of phosphatidylcholine in a monolayer at the air/water interface. Neutron reflection study and reexamination of x-ray reflection experiments. *Biophys. J.* 59:1325-1332.
7. Wiener, M. C. and S. H. White. 1991. Fluid bilayer structure determination by the combined use of x-ray and neutron diffraction. II. "Composition-space" refinement method. *Biophys. J.* 59:174-185.
8. Schalke, M., P. Krüger, M. Weygand, and M. Lösche. 2000. Submolecular organization of DMPA in surface monolayers: Beyond the two-layer model. *Biochim. Biophys. Acta* 1464:113-126.
9. Armen, R. S., O. D. Uitto, and S. E. Feller. 1998. Phospholipid component volumes: Determination and application to bilayer structure calculations. *Biophys. J.* 75:734-744.
10. Kaganer, V. M., H. Möhwald, and P. Dutta. 1999. Structure and phase transitions in Langmuir monolayers. *Rev. Mod. Phys.* 71:779-819.
11. Wu, Y., K. He, S. J. Ludtke, H. W. Huang. 1995. X-ray diffraction study of lipid bilayer membranes interacting with amphiphilic helical peptides: diphytanoyl phosphatidylcholine with alamethicin at low concentrations. *Biophys. J.* 68:2361-2369.
12. Husslein, T., D. M. Newns, P. C. Pattnaik, Q. Zhong, P. B. Moore, and M. L. Klein. 1998. Constant pressure and temperature molecular-dynamics simulation of the hydrated diphytanolphosphatidylcholine lipid bilayer. *J. Chem. Phys.* 109: 2826-2832.
13. Schalke, M. and M. Lösche. 2000. Structural models of lipid surface monolayers from X-ray and neutron reflectivity measurements. *Adv. Colloid Interf.* 88:243-274.
14. Schalke, M., P. Krüger, M. Weygand, and M. Lösche. 2000. Submolecular organization of DMPA in surface monolayers: Beyond the two-layer model. *Biochim. Biophys. Acta* 1464:113-126.
15. Song, L., M. R. Hobaugh, C. Shustak, S. Cheley, H. Bayley, and J. E. Gouaux. 1996. Structure of staphylococcal α-hemolysin, a heptameric transmembrane pore. *Science* 274:1859-1865.
16. Press, W. H., B. P. Flannery, S. A. Teukolsky, and W. T. Vetterling. 1986. Numerical Recipes. Cambridge: Cambridge University Press.